Journal of Power Sources 195 (2010) 1551–1560

Contents lists available at ScienceDirect

Journal of Power Sources

journal homepage: www.elsevier.com/locate/jpowsour

A three-dimensional analysis of the effect of anisotropic gas diffusion layer(GDL) thermal conductivity on the heat transfer and two-phase behavior in a proton exchange membrane fuel cell(PEMFC)

Guangli He [a], Yohtaro Yamazaki [a,*], Abuliti Abudula [b]

[a] Department of Innovative and Engineered Materials, Interdisciplinary Graduate School of Science and Engineering, Tokyo Institute of Technology, Japan
[b] North Japan New Energy Research Center, Hirosaki University, Aomori, Japan

ARTICLE INFO

Article history:
Received 11 June 2009
Received in revised form
29 September 2009
Accepted 29 September 2009
Available online 7 October 2009

Keywords:
PEMFC
Fuel cell
Anisotropic thermal conductivity
GDL
Heat transfer
Two-phase behavior

ABSTRACT

A three-dimensional and two-phase model was employed to investigate the effect of the anisotropic GDL thermal conductivity on the heat transfer and liquid water removal in the PEMFCs with serpentine flow field and semi-counter flow operation. The GDL with different anisotropic thermal conductivity in the three directions (x, y, z) was simulated for four cases. As a result, the water saturation, temperature, species, current, potential distribution and proton conductivity were obtained. According to the comparison between the results of each case, some new conclusions are obtained and listed as below: (1) The anisotropic GDL produces the high temperature difference than that of isotropic case, and the in-plane thermal conductivity perpendicular to the gas channels is more important than that of along channels, which may produce the larger temperature difference. (2) Water saturation decreases due to the large temperature difference in the anisotropic case, but some water vapor may condense in the area neighbor to the channel ribs due to the cool function of the current collector and the great temperature difference. (3) The anisotropic thermal conductivity in the through-plane direction and the in-plane direction perpendicular to the gas channels can lead to the decrease of the membrane conductivity. (4) The isotropic GDL is better than that of anisotropic one for the uniform current density. Also, in-plane thermal conductivity perpendicular to the channels has more negative effect on the current density distribution in the membrane than that of the along channels one.

1. Introduction

Heat management and water management are key issues in the operation of proton exchange membrane fuel cells (PEMFCs), which are well recognized by the researchers. Also, many models and experiments have been done to investigate and optimize the operation to achieve the better water management and good performance of PEMFCs [1–6]. And most of the researches are concentrated on the effect of operating conditions (pressure, flow rate, stoichiometry, humidified level, etc.) on the water removal, however, the heat management also has important effect on the water management due to the closely interacted thermal-mass transfer coupled behavior between water and temperature, also a significant amount of heat is released or absorbed due to the phase change of water, and the rates of which are also a strong function of temperature. Therefore, water management in PEMFCs should be considered with thermal management simultaneously. Hwang [7] developed a two-phase model considering velocity, temperature and current in a PEM fuel cell. He predicted the phase equilibrium front and the thermal equilibrium front in a porous cathode of a PEM fuel cell and concluded that increasing the rib-shoulder temperature will reduce the condensation zones, because the hot rib-shoulder surfaces increase the nearby fluid-phase temperature that increases the saturation pressure. Meng et al. [8] also presented a non-isothermal two-phase model of PEMFCs, and their results indicate a condensation/evaporation interface would appear in the porous materials and its location changes with the inlet humidity value under a low-humidity inlet condition. Also liquid water is mainly produced in the GDL in two regions; one is near the current collecting land owing to the low temperature and another further inside the GDL but still away from the catalyst layer. Falcão et al. [9] recently presented a simple, using low CPU, steady-state, one-dimensional model accounting for coupled heat and mass transfer occurring in a PEM fuel cell. The model outputs are the temperature and concentration across the cell and the water content in the membrane. The model predicts reasonably well the influence of current density and RH on the net water transport coefficient. Humidified cathode and especially humidified anode streams are needed to avoid the membrane dehydration, particularly at high current density. The above researches are based on the isotropic

* Corresponding author. Tel.: +81 45 924 5411.
E-mail address: yamazaki.y.af@m.titech.ac.jp (Y. Yamazaki).

0378-7753/$ – see front matter © 2009 Elsevier B.V. All rights reserved.
doi:10.1016/j.jpowsour.2009.09.059

Nomenclature

a	water activity
C	molar concentration (mol m^{-3})
c_p	specific heat capacity(J kg^{-1} K^{-1})
c_T	mass transfer coefficient (s^{-1})
D	diffusion coefficient (cm^2 s^{-1})
F	Faraday's constant
h_L	latent heat (kJ kg^{-1})
I	current density magnitude (A m^{-2})
i_0^{ref}	reference current density (A m^{-2})
J	reaction rate
K	permeability (cm^2)
k	thermal conductivity (W m^{-1} K^{-1})
M	molar mass (kg mol^{-1})
n	number of electrons
P	pressure (Pa)
R	universal gas constant (J mol^{-1} K^{-1})
S_T	source term in energy equation
S_w	source term in liquid
s	water saturation
T	temperature (K)
V	velocity (cm s^{-1})
V_{oc}	open circuit voltage (V)
y	mass fraction

Greek letters

ϕ	potential (V)
ε	volume fraction
σ	surface tension (N cm^{-1})
σ_{mem}	proton conductivity in membrane
σ_{sol}	electric conductivity of solid
θ_c	equilibrium contact angle on diffuser
λ	polymer water content H_2O/SO_3
α_d	water drag coefficient in membrane
η	overpotential (V)
μ	viscosity (Pa s)
ρ	density (kg cm^{-3})

Subscripts

an	anode
C	about capillary
cat	cathode
sat	Saturated
sol	about electron
g	gas phase
H_2	hydrogen
i	note for species
k	note for phases
l	liquid phase
m	mixture properties of multiphase mixture
mem	polymer phase
O_2	oxygen
ohm	about electronics
p	phase
q	phase
ref	reference
w	water
wv	water vapor

GDL. However the GDL in PEMFCs made of carbon paper which has anisotropic properties such as permeability, thermal conductivity, and electronic conductivity [10]. So the research based on the anisotropic GDL is very necessary.

By now, also some researches are performed to investigate the effect of the anisotropic properties on the performance of PEMFCs [11–17]. The influence of binder structure and PTFE treatment on the anisotropic, effective diffusivity of different carbon paper GDLs has been experimentally investigated for the first time in Reto Flückiger's work [11]. The results revealed a high degree of anisotropy given by the orientation of the fibers is preferable for homogeneous conditions under flow field channel and rib. It is expected to reduce degradation effects caused by local current peaks. Bapat [12] developed a two-dimensional two-phase model to analyze the effects of anisotropic electrical resistivity on current density and temperature distribution in a PEM fuel cell and found that a higher in-plane electrical resistivity of the gas diffusion layer (GDL) adversely affects the current density in the region adjacent to the gas channel and generates slightly higher current densities in the region adjacent to the current collector. He also developed a two-dimensional two-phase model based on the classical two-fluid model to analyze the effect of low through-plane and high in-plane thermal conductivities on the two-phase behavior [13]. It is concluded that the current density may be maximized at low-humidity operating conditions by tailoring the GDL to have high through-plane thermal conductivity near the inlet and progressively decreasing through-plane thermal conductivity at distances farther away from the inlet along the flow channel. Ramousse [14] developed an analytical approach to estimate the thermal conductivity of GDL composed of non-woven carbon felts with anisotropicity. Ju [15] presented two-dimensional simulation to study the effects of gas diffusion layer (GDL) anisotropy and the spatial variation of contact resistance between GDLs and catalyst layers (CLs) on water and heat transfer in polymer electrolyte fuel cells (PEFCs). The simulation results clearly demonstrate that GDL anisotropy and the spatial variation of GDL/CL contact resistance have a strong impact on thermal and two-phase transport characteristics in a PEFC by significantly altering the temperature, water and membrane current density distributions, as well as overall cell performance. Hao [16] developed a multiple-relaxation-time (MRT) lattice Boltzmann method (LBM) to predict the anisotropic permeability of GDL with consideration of porosity and tortuosity. In Yang's work [17], a coupled electron and two-phase mass transport model for anisotropic GDLs is developed. The effects of anisotropic GDL transport properties due to the inherent anisotropic carbon fibers and caused by GDL deformations are studied. Results indicate that the inherent structural anisotropy of the GDL significantly influences the local distribution of both cathode potential and current density. But the heat transfer is not included in their simulation.

Although, some works have been done to consider the anisotropicity of the GDL, most of them are concentrated on the anisotropic permeability, however, the through-plane permeability is not greatly different from the in-plane permeability [10]. But, there is great difference between through-plane thermal conductivity and in-plane thermal conductivity [14,15], so the research of the anisotropic thermal conductivity should be performed due to the importance of the heat management, and only a few references are reported [13,15] which are based on the two-dimensional simulation, and obviously different from the actual PEMFCs. Furthermore, the effect of liquid on the heat transfer is not considered which can be confirmed by the governing equations in their works [15]. Also, the effect of flow field on the heat management, and the difference in the two directions of in-plane thermal conductivity cannot be involved for the two-dimensional cases.

In this study, a two-phase three-dimensional simulation is present for the consideration of the anisotropic thermal conductivity in the three directions (through-plane, in-plane along the channel, in-plane perpendicular to the channel) of the GDLs for the commonly used serpentine flow field with semi-counter flow oper-

ation, and some new conclusions are obtained, which may provide guidelines for the design and operation of PEMFCs. However, gas diffusion is the dominate function in the GDL, and the convection is very weak for the serpentine flow field, so the effect of the mass transfer on the heat transfer is limited and the anisotropic property for mass transfer was not considered.

2. Three-dimensional two-phase simulation

The gas is treated as the ideal gas. Due to the relatively low velocity, the fluid flow is considered as laminar flow. The liquid contact angle of the catalyst layer is 70°. And the effect of the channel wall on the liquid transfer is neglected.

2.1. Governing equations

The continuity equation for the multiphase mixture is

$$\frac{\partial}{\partial t}\rho_m + \nabla\cdot(\rho_m \vec{v_m}) = 0 \tag{1}$$

$$\vec{v_m} = \frac{\sum_{k=1}^{n}(s_k\rho_k\vec{v_k})}{\rho_m}$$
$$\rho_m = \sum_{k=1}^{n}(s_k\rho_k) \tag{2}$$

The momentum equation for the mixture can be expressed as [18]

$$\frac{\partial}{\partial t}(\rho_m\vec{v_m}) + \nabla\cdot(\rho_m\vec{v_m}\vec{v_m}) = -\nabla p + \nabla\cdot[\mu_m(\nabla\vec{v_m}^T + \nabla\vec{v_m})] + \rho_m g + S_{draag}$$

$$\mu_m = \sum_{k=1}^{n}(s_k\mu_k) \tag{3}$$

From the continuity equation for the liquid phase water, the volume fraction equation for liquid water can be obtained:

$$\frac{\partial}{\partial t}(s\rho_l) + \nabla\cdot(\varepsilon s\rho_l\vec{v_m}) = r_w + S_w \tag{4}$$

In the gas diffusion layer and catalyst layer, the liquid is driven by capillary force, then it can be rewritten as

$$\nabla\cdot(\varepsilon s\rho_l\vec{v_m}) = \nabla\cdot\left(\varepsilon s\rho_l\frac{Ks^3}{\mu_l}\nabla p_c\right) = r_w + S_w \tag{5}$$

Capillary pressure is

$$p_C = p_g - p_l = \sigma\ \cos\theta\left(\frac{\varepsilon}{K}\right)^{1/2}J(s) \tag{6}$$

The species mass conservation in gas phase is

$$\nabla\cdot(s_g\rho_g\vec{v}_g y_i) = \nabla\cdot(D_i\nabla y_i) + S_i \tag{7}$$

The membrane phase and solid phase potential conservation equations and electrochemical reaction rate in the cathode side and anode side:

$$\nabla\cdot(\sigma_{mem}\nabla\phi_{mem}) = \begin{cases} J_a & \text{anode catalyst layer} \\ J_c & \text{cathode catalyst layer} \end{cases} \tag{8}$$

$$\nabla\cdot(\sigma_{sol}\nabla\phi_{sol}) = \begin{cases} -J_a & \text{anode catalyst layer} \\ -J_c & \text{cathode catalyst layer} \end{cases} \tag{9}$$

Water motion through the membrane is

$$\nabla\cdot\left(-D_w\nabla C_w + \lambda\frac{2.5i}{22F}\right) = 0 \tag{10}$$

The heat transfer equation is

$$\frac{\partial}{\partial t}(\rho_m c_{p,m}) + \nabla\cdot(\rho_m c_{p,m}\vec{v_m}T) = \nabla\cdot(k_{eff}\nabla T) + S_T \tag{11}$$

Table 1
Sources terms.

Source terms (zero in other region)	Defining equation
Water produced (cathode catalyst layer)	$S_w = J_c\frac{M_{H_2O}}{2F}$
Darcy pressure drop of gas in cathode and anode, S_{Drag}	$-\varepsilon\left(\frac{\mu_g}{K(1-s)^3} + \frac{\mu_l}{Ks^3}\right)\vec{v_m}$
Oxygen reaction rate (cathode catalyst layer)	$S_{O_2} = -J_c\frac{M_{O_2}}{4F}$
Hydrogen reaction rate (anode catalyst layer)	$S_{H_2} = -J_a\frac{M_{H_2}}{2F}$
Mass transfer rate between gas and liquid	$r_w = c_T\max\left(\left[(1-s)\frac{p_{wv}-p_{sat}}{RT}M_w\right], [-s\rho_l]\right)$
Energy source term	$S_T = I^2R_{ohm} + \eta_{an,cat}J_{an,cat} + r_w h_L$

where

$$T = \sum_{k=1}^{n}\frac{s_k\rho_k T_k}{\rho_m}$$
$$k_{eff} = \varepsilon\sum_{k=1}^{n}s_k k_k + (1-\varepsilon)k_s \tag{12}$$
$$\rho_m c_{pm} = \sum_{k=1}^{n}\rho_k c_{p,}$$

For the anisotropic GDL, the thermal conductivity can be described as

$$k_{GDL} = k\begin{Bmatrix} xx & 0 & 0 \\ 0 & yy & 0 \\ 0 & 0 & zz \end{Bmatrix} \tag{13}$$

xx, *yy*, and *zz* are the direction vectors.

The source terms and parameters in the equations are listed in Tables 1 and 2.

2.2. Boundary conditions and parameters

The simulation domain is shown in Fig. 1, which includes the current collector, gas channel, gas diffusion layer, catalyst layer both in anode side and cathode side, and membrane, also the inlet and outlet for the anode and cathode are schematically shown in Fig. 1. The conventional serpentine flow field is investigated in the present study (shown in Fig. 2), which has 17 channels. And the size of the PEMFC is 5 cm × 3.3 cm.

The inlet volume flow rate is 500 ml min^{-1}, which is converted to mass flow rate by the UDF (user defined function in Fluent® software), the outlet boundary condition is the pressure outlet condition, the outlet pressure is equal to atmosphere pressure. The operation current density is 1.0 A cm^{-2}. The inlet temperature is

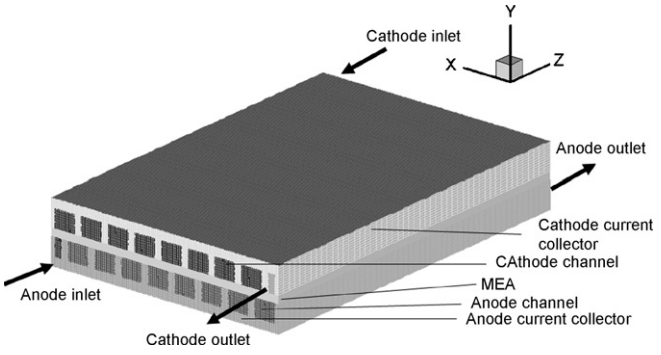

Fig. 1. Calculation domain.

Table 2
Parameters.

Parameters	Defining equation
Reaction rate in cathode CL	$J_c = (1-s)A_v i_{0,c}^{ref}\left(\frac{C_{O_2}}{C_{O_2}^{ref}}\right)\left[\exp\left(\frac{-n\alpha_a}{RT}(\phi_{mem}+\phi_{sol}-V_{oc})\right)-\exp\left(\frac{n\alpha_c}{RT}(\phi_m+\phi_{sol}-V_{oc})\right)\right]$
Reaction rate in anode CL	$J_a = (1-s)A_v i_{0,a}^{ref}\left(\frac{C_{H_2}}{C_{H_2}^{ref}}\right)\left[\exp\left(\frac{-n\alpha_a}{RT}(\phi_{sol}-\phi_{mem})\right)-\exp\left(\frac{n\alpha_c}{RT}(\phi_{sol}-\phi_{mem})\right)\right]$
Polymer phase conductivity	$\sigma_{mem} = \varepsilon_{mem}(5.14\lambda - 3.26)\exp\left[1268\left(\frac{1}{303}-\frac{1}{T}\right)\right]\ (\lambda > 1)$
Water content in polymer phase	$C_w = \frac{e\lambda}{j\lambda+1}$
Water index in polymer	$\lambda = 0.043 + 17.81a - 39.85a^2 + 36.0a^3 \quad a < 1$ $\lambda = 14 + 1.4(a-1) \quad a \geq 1$
Water activity	$a = \frac{p_{wv}}{p_w^{sat}} + 2s$
Water diffusivity in polymer phase	$D_w = 10^{-10}\exp\left[2416\left(\frac{1}{303}-\frac{1}{T}\right)\right](2.563 - 0.33\lambda + 0.0264\lambda^2 - 0.000671\lambda^3) \quad \lambda > 4$ $D_w = 10^{-10}\exp\left[2416\left(\frac{1}{303}-\frac{1}{T}\right)\right](-1.25\lambda + 6.65) \quad 3 < \lambda \leq 4$ $D_w = 10^{-10}\exp\left[2416\left(\frac{1}{303}-\frac{1}{T}\right)\right](2.05\lambda - 3.25) \quad 2 < \lambda \leq 3$ $D_w = 10^{-10}\exp\left[2416\left(\frac{1}{303}-\frac{1}{T}\right)\right] \quad \lambda \leq 2$
The effective diffusion coefficient [19]	$D_i = \varepsilon^{1.5}(1-s)^{2.5}D_{i,0}\left(\frac{p_0}{p}\right)\left(\frac{T}{T_0}\right)^{1.5}$
Leverett J-function	$J(s) = \begin{cases} 1.417(1-s) - 2.120(1-s)^2 + 1.263(1-s)^3 & \text{if } \theta_C < 90^\circ \\ 1.417s - 2.120s^2 + 1.263s^3 & \text{if } \theta_C > 90^\circ \end{cases}$
Saturated water vapor pressure	$\log_{10}^{p_{sat}} = -2.1794 + 0.02953(T-273.17) - 9.1837\times10^{-5}(T-273.17)^2 + 1.4454\times10^{-7}(T-273.17)^3$

353 K, and the temperature of anode current collector and cathode current collector end walls boundary are the 353 K, which means the current collector is ideally cooled to keep constant temperature. The other lateral walls and the end walls are impermeable for all the species. The potential on the anode current collector boundary is set to be 0. The water saturation in cathode and anode inlet are zero. The inlet gas for anode side and cathode side are humidified at 348 K before entering the PEMFCs.

The values of the other parameters used in the model are listed in the Table 3.

2.3. Mesh grid and solution technique

The geometry model shown in Fig. 1 was discretized into 660,000 hexahedral mesh volumes, and to assure the quality of the grid, the size of the grid in gas channel, gas diffusion layer, catalyst layer and membrane are different. The simple algorithm is applied for solving the pressure–velocity coupled equations, and species equations. And suitable relax factors are used for water saturation, potential and water content. The simulation is performed in Flunet®6.3 software of Ansys company with the additional UDFs(User Defined Function in Fluent) developed by the authors.

3. Results and discussion

To investigate the effect of the anisotropic GDL on the heat and water management, the simulations for four cases are completed. The conditions of the four cases are listed in Table 4. And the typical anisotropic values of the thermal conductivity in GDL are obtained in Refs. [20,14,15].

The through-plane thermal conductivity of GDL is obtained in Refs. [20,14], which is great smaller than that of the in-plane case, this is determined by the structure of the carbon paper. In common case, the carbon paper is composed of random packed carbon fibers, and the heat transfer in the through-plane mainly occurs between the different carbon fibers, furthermore, there is also space between the carbon fibers, so the thermal conductivity is weak. As for the heat transfer in the in-plane direction, the heat transfer is mainly accomplished in the same carbon fiber, so the thermal conductivity is larger than that of through-plane case, and that means the in-plane thermal conductivity is determined by the orientation and length of the carbon fibers. So, the thermal conductivity in the in-plane can also be different. In the present study, case 3 and case 4 are designed to consider this point. In case 3, it means that all of the carbon fibers are orientated to the in-plane direction perpendicular to the gas channel, and case 4 means all of the carbon fibers are orientated to the in-plane direction along the gas channel. So, the thermal conductivity in the other directions is the same as the through-plane one. By this way, the effect of anisotropic thermal conductivity in GDL on the heat transfer is related to the structure of the flow field.

3.1. The effect of anisotropic thermal conductivity on the temperature

Figs. 3–6 show the temperature distribution on the cathode catalyst layer–membrane surface for the four different cases. Com-

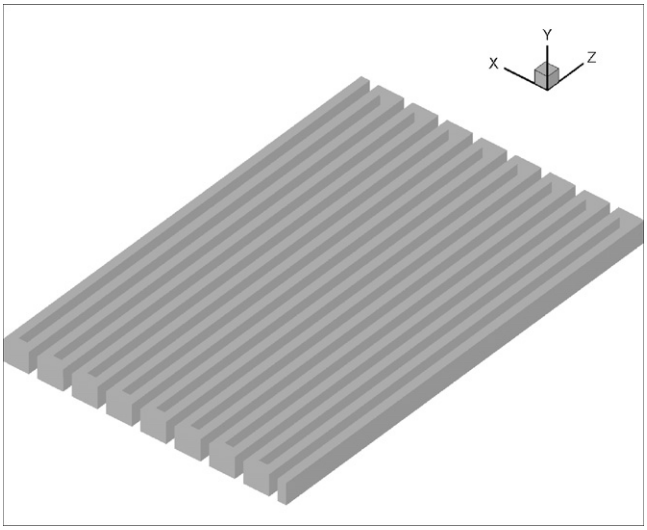

Fig. 2. Schematic view of the flow field.

Table 3
Values of the parameters.

Physical properties	Value
Faraday's constant, F	96487 C mol^{-1}
Permeability of gas diffusion layer, K	8×10^{-8} cm^2
Liquid water viscosity, μ_l	3.565×10^{-4} Pa s
Anodic/cathodic transfer coefficient,α_a/α_c	0.5/0.55
Water contact angle in diffuser, θ	120°
Gas channel width	0.1 cm
Gas channel height	0.1 cm
Thickness of current collector	0.15 cm
Anode GDL thickness	0.019 cm
Cathode GDL thickness	0.019 cm
Gas diffusion layer void fraction	0.78
Catalyst layer thickness	0.002 cm
Catalyst layer void fraction	0.5
Membrane thickness (Nafion® 112)	0.0005 cm
Cell Inlet temperature	353 K
Outlet pressure	0.1 MPa
Air and fuel inlet humidified temperature	348 K
Open circuit voltage	0.95 V
Mass transfer rate between phases, c_T	100 s^{-1}
Gas constant, R	8314 J kmol^{-1} K^{-1}
Reference hydrogen concentration, $C^{ref}_{H_2}$	1 kmol m^{-3}
Reference oxygen concentration, $C^{ref}_{O_2}$	1 kmol m^{-3}
Operation current density	1.0 A cm^{-2}
Anode exchange current density, $i^{ref}_{0,a}$	1.5e8 A m^{-3}
Cathode exchange current density, $i^{ref}_{0,c}$	7000 A m^{-3}
Thermal conductivity of catalyst layer [20]	0.27 W m^{-1} K^{-1}
Thermal conductivity of membrane [20]	0.29 W m^{-1} K^{-1}
Specific heat capacity of membrane	800 J kg^{-1} K^{-1}
Specific heat capacity of GDL	1000 J kg^{-1} K^{-1}
Specific heat capacity of catalyst layer	1000 J kg^{-1} K^{-1}
Specific heat capacity of current collector	800 J kg^{-1} K^{-1}
Specific heat capacity of air	1006.43 J kg^{-1} K^{-1}
Specific heat capacity of hydrogen	14283 J kg^{-1} K^{-1}

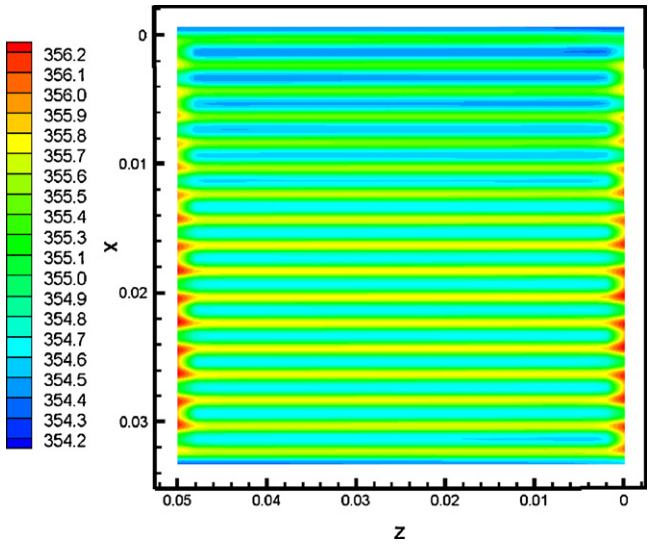

Fig. 3. Temperature on the cathode catalyst layer–membrane interface for case 1, K (x:m, z:m).

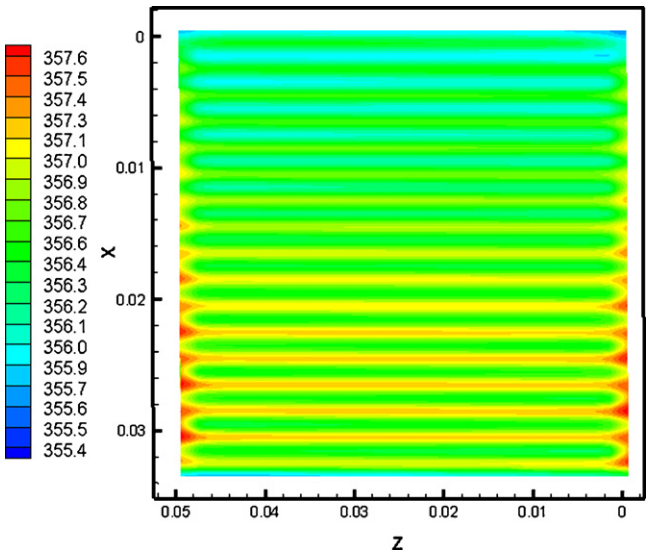

Fig. 4. Temperature on the cathode catalyst layer–membrane interface for case 2, K (x:m, z:m).

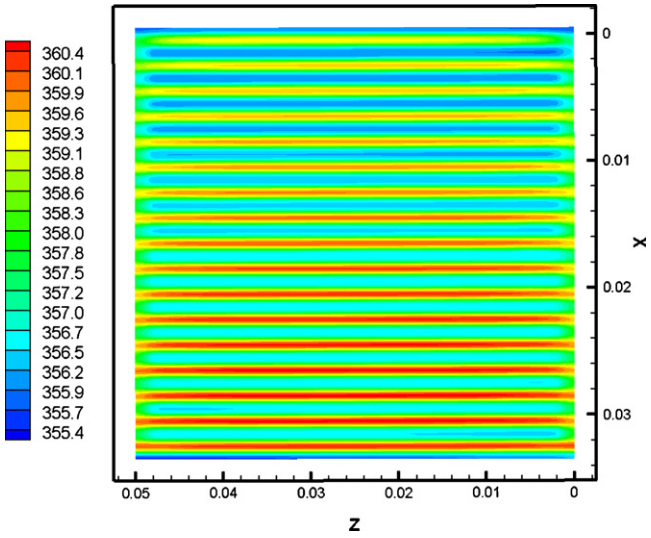

Fig. 5. Temperature on the cathode catalyst layer–membrane interface for case 3, K (x:m, z:m).

pared with the temperature for the isotropic case, it is obvious that the maximum temperature for all the anisotropic cases (357.6 °C, 360.4 °C, and 357.8 °C separately) are larger than the maximum temperature for the isotropic case (356.4 °C). This is due to the weak thermal conductivity of the anisotropic cases (the thermal conductivity for the isotropic case in the through-plane is nearly 10 times of that for the anisotropic cases). The maximum temperatures are also different for the different anisotropic cases. And according to the result in Figs. 4–6, there is great difference for the temperature distribution for the different anisotropic cases. The largest

Table 4
Different thermal conductivity for the simulation.

	Through-plane thermal conductivity (y) (W m^{-1} K^{-1})	In-plane thermal conductivity along channels (z) (W m^{-1} K^{-1})	In-plane thermal conductivity perpendicular to the channels (x) (W m^{-1} K^{-1})
Case 1	10 [15]	10	10
Case 2	1.27 [14,20]	10	10
Case 3	1.27	10	1.27
Case 4	1.27	1.27	10

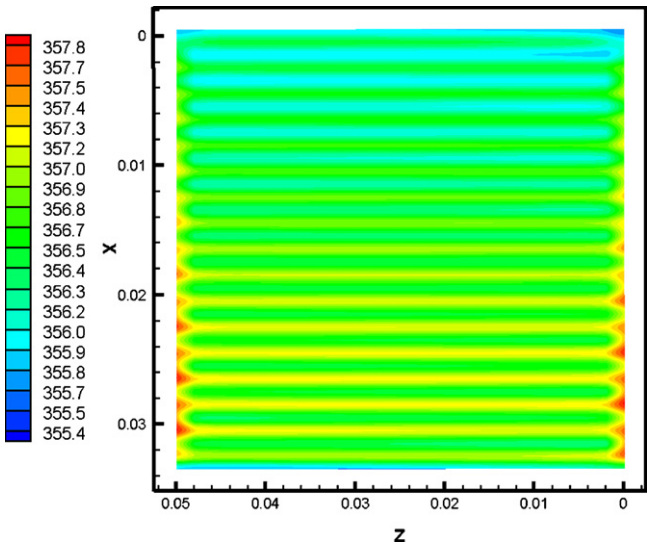

Fig. 6. Temperature on the cathode catalyst layer–membrane interface for case 4, K (*x*:*m*, *z*:*m*).

temperature difference between the area neighbor to the channel area and the area neighbor to the ribs is obtained in case 3. This is caused by the heat in the area neighbor to the channel area is hard to transfer due to the weak thermal conductivity in the *x* direction, which makes the temperature increase sharply. However, For case 2 and case 4, the temperature distribution including the maximum temperature are nearly the same (357.6 °C and 357.8 °C for the maximum temperature). That means the weak in-plane along-channel thermal conductivity has little effect on the heat transfer in the fuel cells. However, all the operation conditions and the properties of the material are the same for case 3 and case 4, and the only difference is the direction of the weak thermal conductivity, for case 3, through plane of and in-plane perpendicular to the gas channel thermal conductivities are weak, while the weak thermal conductivity are in through plane of GDL and in-plane along the gas channel (except the corner) for case 4. In the present fuel cell, the heat produced in the operation is removed in the following ways: firstly, the heat is removed through the anode and cathode current collector which neighbors the cool plate in the actual application, the function of the cool plate is described by the constant temperature on the current collector-cool plate interface (end walls of current collector) in the present study. In this case, the heat transfer mainly happened in the direction of through plane, but there is no difference between case 3 and case 4 related to that, so the heat transfer in this way should also be the same. The second way of heat removal is heat removed by the reactant gas, which flows in fuel cell and flows out carrying the excessive heat. Because of the higher thermal conductivity of the current collector compared to that of the reacting gases, heat can be easily removed from the current collector, so the temperature in the area near the ribs of the current collector is low compared to that of the area near the channel, which can be demonstrated by all the simulation temperature distribution. For case 3, the in-plane thermal conductivity perpendicular to the gas channel is weak, that means the heat transfer from the GDL area near gas channels to the GDL area near ribs is hard, and the heat transfer ability in the area near gas channels is also low due to the weak thermal conductivity and the limit flow rate of the gases. So, the produced heat cannot be removed efficiently, which causes the high temperature near the channels and the great temperature difference between area near channels and area near ribs. In other words, in-plane thermal conductivity perpendicular to the gas channels is very important for the heat transfer in the PEMFCs.

As for the case 4, the weak thermal conductivities are through-plane and in-plane along-channel thermal conductivities. But there is little difference between the results of case 2 and case 4. That means the heat transfer is mainly accomplished in the through-plane direction and in-plane direction perpendicular to the gas channels, so the in-plane thermal conductivity along the gas channels is not important, and has limited effect on the heat transfer in the PEMFCs. So, it can be concluded that the anisotropic GDL produces the high temperature difference than that of isotropic case, and the in-plane conductivity perpendicular to the gas channels is more important than that of along channels, and the anisotropic thermal conductivity in this direction may produce the even larger temperature difference.

3.2. The effect of anisotropic thermal conductivity on the water saturation in cathode GDL and catalyst layer

Figs. 7–10 show the water saturation in cathode catalyst layer and gas diffusion layer in the cross-section ($z = 0.025$ cm) of the PEMFC. It can be seen that the maximum water saturation for the isotropic case is about 0.07, while the maximum value for the other cases are about 0.05. According to the analysis in the Section 3.1 that the isotropic GDL has the low temperature, that means low saturated water vapor concentration, so less water produced by the electrochemical reaction can vaporize to the water vapor compared with the other cases, and more water remains in liquid which leads to the high water saturation. In other words, the anisotropic GDL decreases the water saturation in the cathode catalyst layer and GDL.

It is well known that the liquid water flows through the catalyst layer and GDL is driven by the capillary force, and there is water saturation gradient through the thickness of the catalyst layer and

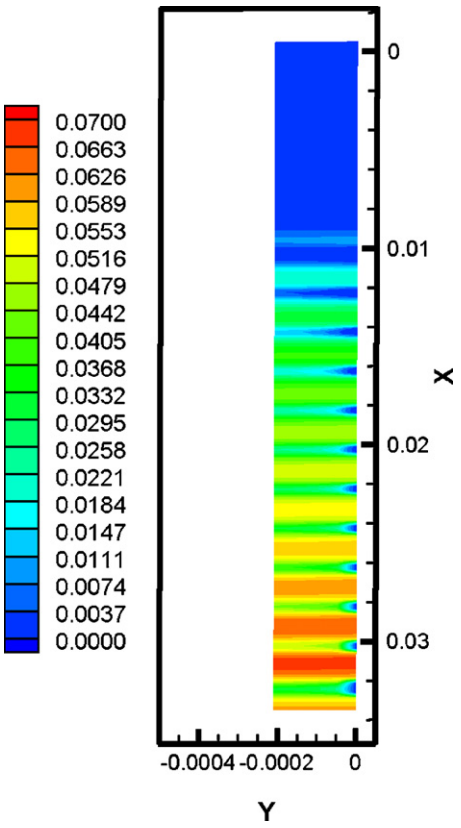

Fig. 7. Water saturation in the cross-section of $z = 0.025m$ of cathode GDL and catalyst layer for case 1 (*x*:*m*, *z*:*m*).

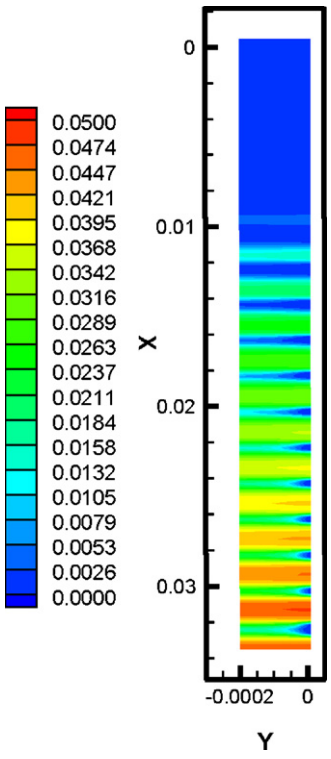

Fig. 8. Water saturation in the cross-section of $z = 0.025m$ of cathode GDL and catalyst layer for case 2 (x:m, z:m).

the GDL, i.e. water saturation increases from GDL-channel surface to the catalyst layer surface, which is confirmed by many simulation results. And, the present simulation results for the isotropic GDL also show the same trend with described above which can be seen in Fig. 7. But, as for the result for the other three cases, it is

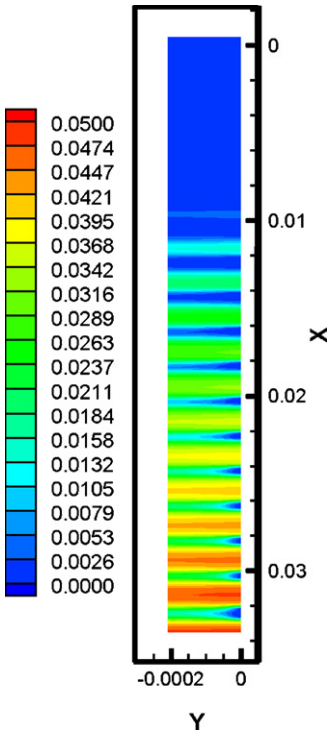

Fig. 9. Water saturation in the cross-section of $z = 0.025m$ of cathode GDL and catalyst layer for case 3 (x:m, z:m).

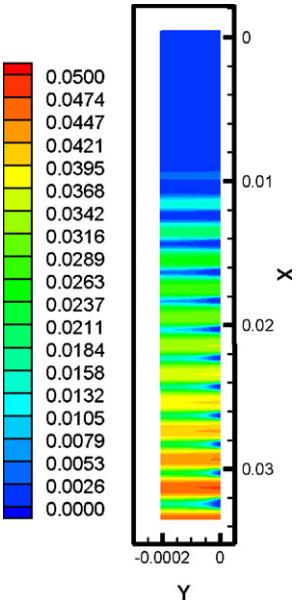

Fig. 10. Water saturation in the cross-section of $z = 0.025m$ of cathode GDL and catalyst layer for case 4 (x:m, z:m).

different. It can be seen that there are relative high water saturation areas neighbor to the current collector's ribs, not only in the catalyst layer in Figs. 8 and 10 for case 2 and case 4, but also more obvious in Fig. 9 for case 3, that means water saturation neighbor to the ribs is larger than that of the area neighbor to the catalyst layer, and the motion of the water is not mainly determined by the capillary force, there is also something else: temperature. According to the results in Figs. 3–6, the temperature in the catalyst layer and GDL of case 2, case 3 and case 4 are higher than that of case 1 both for the area neighbor to the ribs and neighbor to the channel. So, more liquid water vaporizes to water vapor in those three cases in the catalyst layer near the channels, and the water vapor in the area neighbor to the gas channel can directly enter into the gas channel and flows out, which makes the water saturation decrease from the catalyst layer to the gas channel, as for the water in the area neighbor to the ribs, also more water vaporizes to water vapor in the catalyst layer due to the relative high temperature, but there is long distance from this area to the gas channels, which leads to the high flow resistance compared with the former one, furthermore the temperature in the area neighbor to the ribs is low due to the good heat removal performance of the current collector, which makes some water vapor from the catalyst layer condense in the area neighbor to the ribs, so the water saturation increases from catalyst layer to the GDL. So, it can be concluded that water saturation decreases due to the large temperature difference in the anisotropic case, and some water vaporized in the catalyst layer because of the high temperature for anisotropic cases, but some water vapor condenses in the area neighbor to the ribs due to the well cool function of the current collector, which cause the water saturation in the area neighbor to the ribs is larger than that of in the catalyst layer.

3.3. *The effect of anisotropic thermal conductivity on the proton conductivity*

The proton conductivity of the membrane is determined by the water content and temperature in the membrane, high temperature and high water content are helpful to the proton conductivity. According to the analysis before, the temperature increases due to the anisotropic thermal conductivity in the GDL, but as the tem-

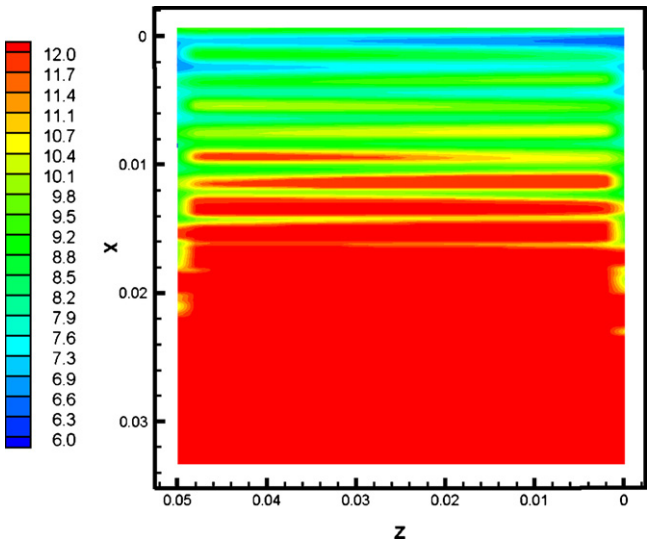

Fig. 11. Proton conductivity on the cathode side of the membrane for case 1, S m^{-1} (x:m, z:m).

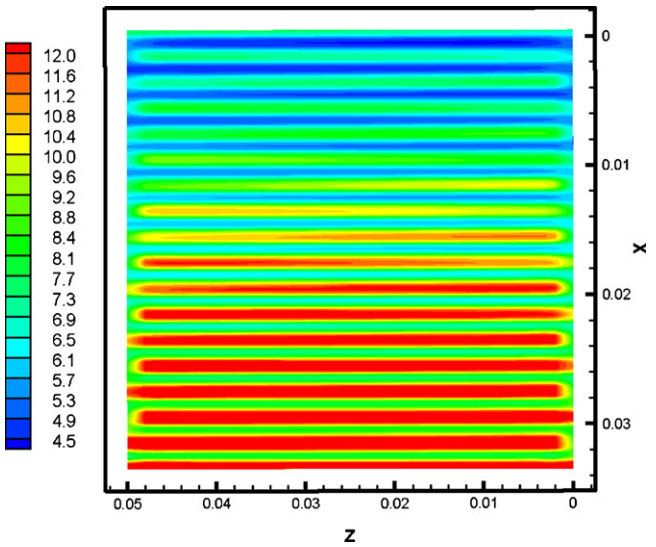

Fig. 13. Proton conductivity on the cathode side of the membrane for case 3, S m^{-1} (x:m, z:m).

perature increases, some liquid water vaporized to water vapor, so the water saturation for the anisotropic case decreases according to the conclusion in Section 3.2. To investigate the effect of the anisotropic thermal conductivity on the performance of the membrane, the proton conductivity on the membrane–cathode surface for the different cases is shown in Figs. 11–14. It can be easily seen that the proton conductivity of the case 3 (maximum value is 12.0, and the minimum value is 4.5) is smaller than that of case 2 and case 4 (maximum value is 12.0, and the minimum value is 5.0). As for the case 1 (the isotropic case), the maximum value is 12.0, while the minimum value is 6.0. Also, the average proton conductivity of the membrane for the four cases is obtained and shown in Fig. 15. It can be easily seen that the highest proton conductivity is in case 1 and lowest proton conductivity is in case 3, while the proton conductivity for case 2 and case 4 are nearly the same, which are higher than that of case 3 and lower than that of case 1. So, the best membrane performance is obtained for isotropic GDL, and the conclusion can be drawn as: the anisotropic thermal conductivity in the through-plane direction and the in-plane direction perpendic-

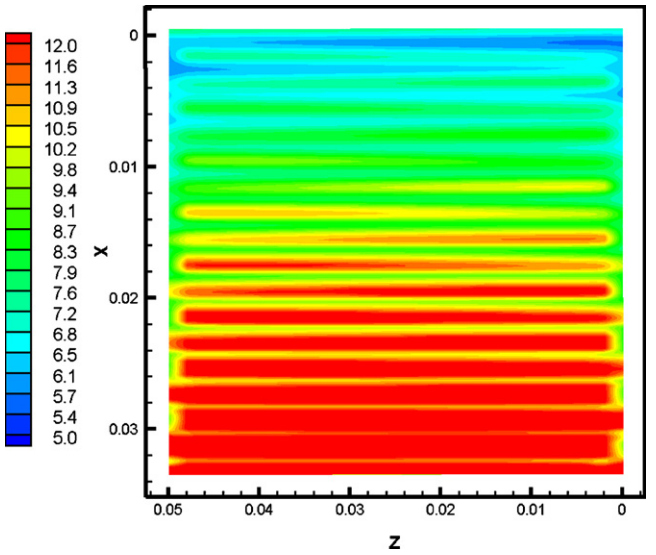

Fig. 14. Proton conductivity on the cathode side of the membrane for case 4, S m^{-1} (x:m, z:m).

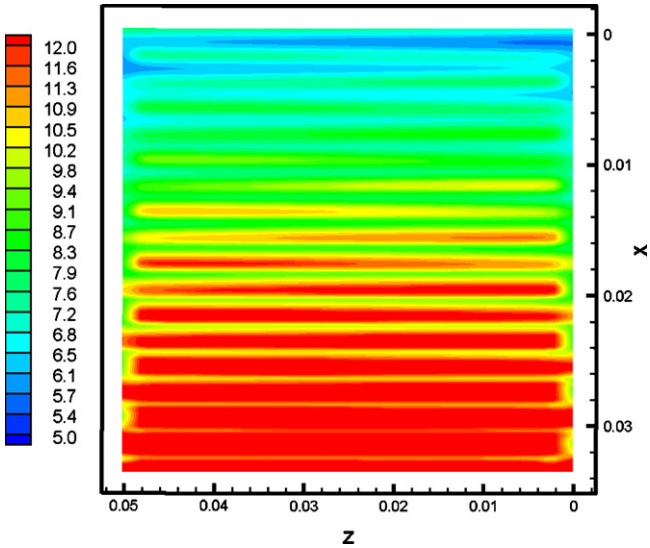

Fig. 12. Proton conductivity on the cathode side of the membrane for case 2, S m^{-1} (x:m, z:m).

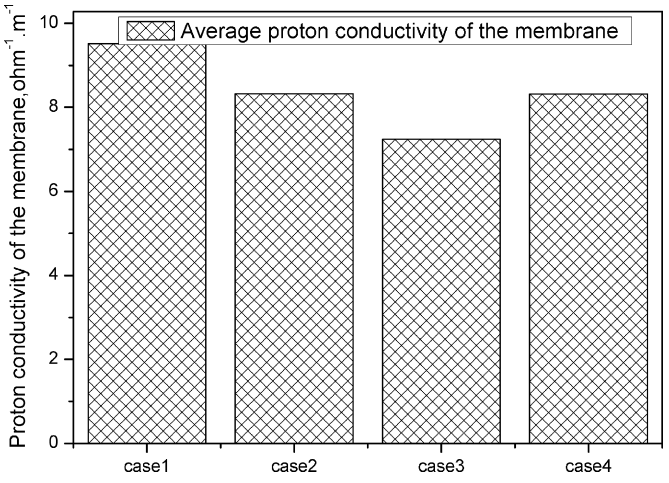

Fig. 15. Comparison between the average proton conductivity of the membrane for four cases.

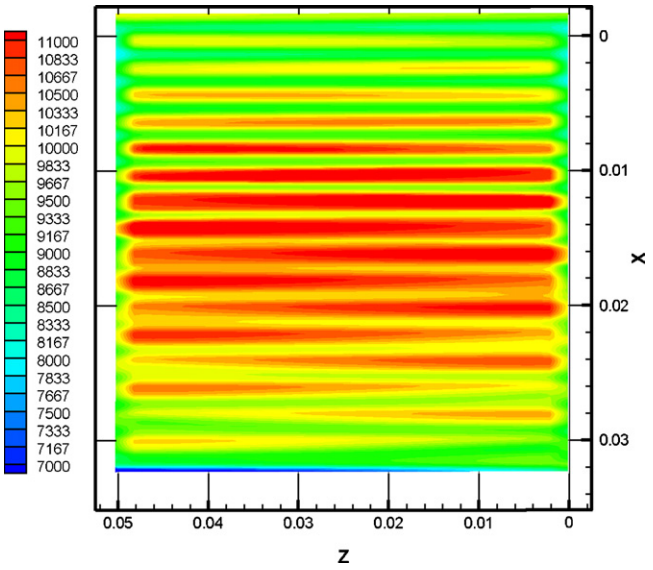

Fig. 16. The current density in the middle membrane for the case 1, A m^{-2} (x:m, z:m).

ular to the gas channels can lead to the decrease of the membrane performance.

3.4. The effect of the anisotropic thermal conductivity on the current density in the membrane

Figs. 16–19 show the current density in the middle membrane for the four cases. It can be seen that the range of current density in the membrane for the isotropic case is smaller than that of other three cases, and the current density difference between the area near the ribs and the area near channels for the isotropic case is also smaller than that of the other three cases. The current density distribution in the middle area of first case in Fig. 16 is nearly uniform, but for the other three cases, the difference is very obvious, especially for the third case. And the distribution for the case 2 and case 4 are nearly same. In the operation of PEMFCs, the uniform current density distribution is pursued due to the non-uniform current density may cause the distortion and other things. So, in the view of this point, the isotropic GDL is better than that of anisotropic one. Also, in-plane thermal conductivity perpendicular to the channels has more negative effect on the current density distribution in the membrane than that of the along channels one.

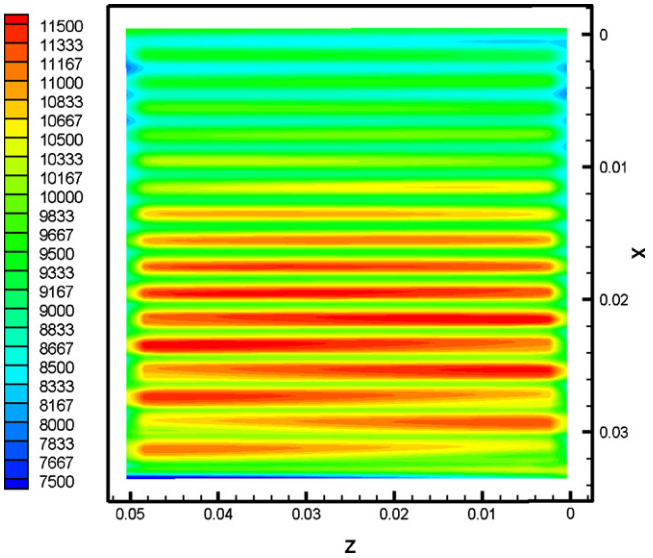

Fig. 17. The current density in the middle membrane for the case 2, A m^{-2} (x:m, z:m).

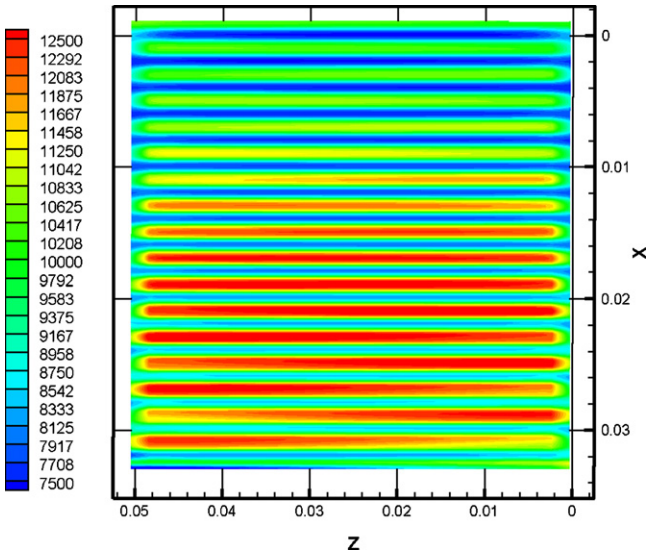

Fig. 18. The current density in the middle membrane for the case 3, A m^{-2} (x:m, z:m).

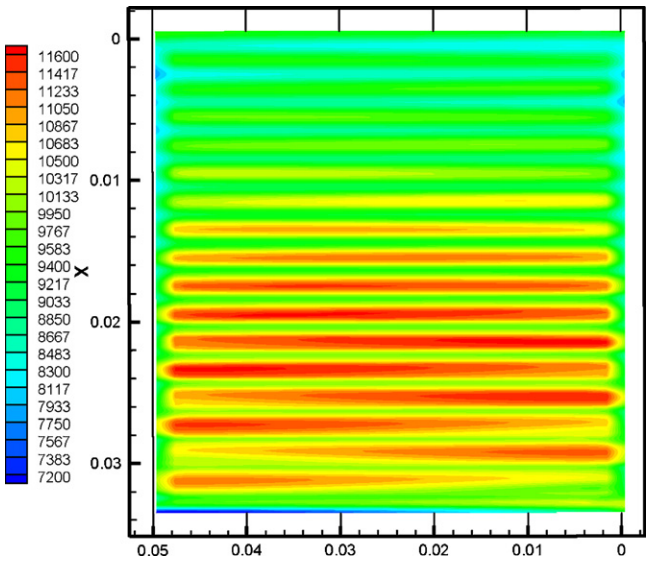

Fig. 19. The current density in the middle membrane for the case 4, A m^{-2} (x:m, z:m).

4. Conclusions

In this paper, a three-dimensional and two-phase model was employed to investigate the effect of the anisotropic GDL thermal conductivity on the heat transfer and liquid water removal in the PEMFCs with serpentine flow field and semi-counter flow operation. The GDL with different anisotropic thermal conductivity in the three directions (x, y, z) was simulated in four cases i.e. case 1 (isotropic thermal conductivity with the good thermal conductivity in every direction), case 2 (anisotropic through-plane thermal conductivity, which means the carbon fibers are packed in the through-plane direction, so the thermal conductivity in this direction is weak), case 3 (anisotropic thermal conductivity in through-plane direction and in-plane direction perpendicular to

the gas channel, which means all the packed carbon fibers are orientated to the along-channel direction, so the thermal conductivity in the other two directions are weak), case 4 (anisotropic thermal conductivity in through-plane direction and in-plane direction along to the gas channel, which means all the packed carbon fibers are orientated to the direction perpendicular to the gas channel, so the thermal conductivity in the other two directions are weak). As a result, the water saturation, temperature, species, current, potential distribution, water content, proton conductivity, etc. were obtained. The effect of the anisotropic thermal conductivity was investigated by the comparison between the results of the temperature, water saturation, proton conductivity and outlet water ratio for the four cases. And the results show that:

(1) The anisotropic GDL produces the high temperature difference than that of isotropic case, and the in-plane thermal conductivity perpendicular to the gas channels is more important than that of along channels. The anisotropic thermal conductivity in this direction may produce the larger temperature difference.
(2) Water saturation decreases due to the large temperature difference in the anisotropic case, and some liquid water vaporizes in the catalyst layer because of the high temperature for anisotropic cases, but some water vapor condenses in the area neighbor to the ribs due to the well cool function of the current collector especially for the anisotropic cases, which makes the water saturation neighbor to the ribs is larger than that of the catalyst layer.
(3) The anisotropic thermal conductivity in the through-plane direction and the in-plane perpendicular to the gas channels direction can lead to the decrease of the membrane performance.
(4) In the view of current density distribution in the membrane, the isotropic GDL is better than that of anisotropic one. Also, in-plane thermal conductivity perpendicular to the channels has more negative effect on the current density distribution in the membrane than that of the along channels one.

These conclusions provide the new guidelines for the design of GDL and operation of PEMFCs.

References

[1] P.K. Sinha, P. Halleck, C.-Y. Wang, Electrochem. Solid-State Lett. 9 (2006) A344–A348.
[2] F.Y. Zhang, X.G. yang, C.Y. Wang, J. Electrochem. Soc. 153 (2006) A225–232.
[3] E. Kimball, T. Whitaker, I.G. Kevrekidis, J.B. Benziger, ECS Trans. 11 (2007) 725–736.
[4] E. Kimball, T. Whitaker, Y.G. Kevrekidis, J.B. Benziger, AIChE J. 54 (2008) 1313–1332.
[5] H. Masuda, K. Ito, T. Oshima, K. Sasaki, J. Power Sources 177 (2008) 303–313.
[6] G. He, P. Ming, Z. Zhao, A. Abudula, Y. Xiao, J. Power Sources 163 (2007) 864–873.
[7] J.J. Hwang, J. Power Sources 164 (2007) 174–181.
[8] H. Meng, J. Power Sources 168 (2007) 218–228.
[9] D.S. Falcão, V.B. Oliveira, C.M. Rangel, C. Pinho, A.M.F.R. Pinto, Chem. Eng. Sci. 64 (2009) 2216–2225.
[10] M. Mathias, J. Roth, F. Jerry, et al., Handbook of Fuel Cells—Fundamentals Technology and Applications, John Wiley & Sons, Ltd., 2003.
[11] R. Flückiger, S.A. Freunberger, D. Kramer, Electrochim. Acta 54 (2008) 551–559.
[12] C.J. Bapat, S.T. Thynell, J. Power Sources 185 (2008) 428–432.
[13] C.J. Bapat, S.T. Thynell, J. Power Sources 179 (2008) 240–251.
[14] J. Ramousse, S. Didierjean, O. Lottin, D. Maillet, Int. J. Therm. Sci. 47 (2008) 1–6.
[15] H. Ju, J. Power Sources (2009), doi:10.1016/j.jpowsour.2009.01.103.
[16] L. Hao, P. Cheng, J. Power Sources 186 (2009) 104–114.
[17] W.W. Yang, T.S. Zhao, Y.L. He, J. Power Sources 185 (2008) 765–775.
[18] A. Dinh Le, B. Zhou, J. Power Sources 182 (2008) 197–222.
[19] P.K. Sinha, C.-Y. Ay Su, Int. J. Hydrogen Energy 32 (2007) 886–894.
[20] M. Khandelwal, M.M. Mench, J. Power Sources 161 (2006) 1106–1115.